International Journal of Nanomedicine

Dovepress
open access to scientific and medical research

Open Access Full Text Article

ORIGINAL RESEARCH

# Iron Oxide Nanoparticles Combined with Cytosine Arabinoside Show Anti-Leukemia Stem Cell Effects on Acute Myeloid Leukemia by Regulating Reactive Oxygen Species

This article was published in the following Dove Press journal:
*International Journal of Nanomedicine*



Jun Dou[1,*]
Luoyang Li[1,*]
Mei Guo[1,*]
Feng Mei[1]
Danfeng Zheng[1]
Hui Xu[1]
Rui Xue[1]
Xueyang Bao[1]
Fengshu Zhao[1]
Yu Zhang[2]

[1]Department of Pathogenic Biology and Immunology, Medical College, Southeast University, Nanjing, 210009, People's Republic of China; [2]State Key Laboratory of Bioelectronics, Jiangsu Key Laboratory for Biomaterials and Devices, School of Biological Science and Medical Engineering, Southeast University, Nanjing, 210009, People's Republic of China

*These authors contributed equally to this work

Correspondence: Jun Dou
Department of Pathogenic Biology and Immunology, Medical School, Southeast University, Nanjing, 210009, People's Republic of China
Email njdoujun@seu.edu.cn

Yu Zhang
School of Biological Science and Medical Engineering, Southeast University, Nanjing, 210009, People's Republic of China
Email zhangyu@seu.edu.cn

**Background and Aim:** Acute myeloid leukemia (AML), initiated and maintained by leukemia stem cells (LSCs), is often relapsed or refractory to therapy. The present study aimed at assessing the effects of nanozyme-like $Fe_3O_4$ nanoparticles (IONPs) combined with cytosine arabinoside (Ara-C) on LSCs in vitro and in vivo.

**Methods:** The $CD34^+CD38^-$LSCs, isolated from human AML cell line KG1a by a magnetic activated cell sorting method, were treated with Ara-C, IONPs, and Ara-C+ IONPs respectively in vitro. The cellular proliferation, apoptosis, reactive oxygen species (ROS), and the related molecular expression levels in LSCs were analyzed using flow cytometry, RT-qPCR, and Western blot. The nonobese diabetic/severe combined immune deficiency mice were transplanted with LSCs or non-LSCs via tail vein, and then the mice were treated with Ara-C, IONPs and IONPs plus Ara-C, respectively. The therapeutic effects on the AML bearing mice were further evaluated.

**Results:** LSCs indicated stronger cellular proliferation, more clone formation, and more robust resistance to Ara-C than non-LSCs. Compared with LSCs treated with Ara-C alone, LSCs treated with IONPs plus Ara-C showed a significant increase in apoptosis and ROS levels that might be regulated by nanozyme-like IONPs via improving the expression of pro-oxidation molecule gp91-phox but decreasing the expression of antioxidation molecule superoxide dismutase 1. The in vivo results suggested that, compared with the AML bearing mice treated with Ara-C alone, the mice treated with IONPs plus Ara-C markedly reduced the abnormal leukocyte numbers in peripheral blood and bone marrow and significantly extended the survival of AML bearing mice.

**Conclusion:** IONPs combined with Ara-C showed the effectiveness on reducing AML burden in the mice engrafted with LSCs and extending mouse survival by increasing LSC's ROS level to induce LSC apoptosis. Our findings suggest that targeting LSCs could control the AML relapse by using IONPs plus Ara-C.

**Keywords:** acute myeloid leukemia, leukemia stem cells, $Fe_3O_4$ nanoparticles, cytosine arabinoside, reactive oxygen species

## Introduction

Acute myeloid leukemia (AML) accounts for approximately 30% of leukemia cases, it is the most frequently diagnosed type of acute leukemia in the elderly, and its drug-resistant relapse is common.[1,2] The disease is characterized by abnormal primitive medullary system cell proliferation, poor cell differentiation, and infiltration of bone marrow, peripheral blood, and other tissues such as liver, spleen,

and lymph nodes. AML patients are also found to have common hematopoiesis suppression, white blood cell abnormality in qualitative nature and quantity, and decrease in erythrocytes and platelets. Currently, standard care methods for AML treatment include new chemotherapeutic drugs, such as a combination of cytosine arabinoside (Ara-C) with an anthracycline to improve the curative effect and prolong the survival of patients. However, many patients still ultimately relapsed due to occurrence of drug resistance, although two-thirds of AML patients achieve complete remission with progression-free survival. Therefore, AML chemotherapy resistance is still a major challenge in the treatment of AML.

Leukemia stem cells (LSCs), a very small subpopulation of the total number of leukemic cells, are considered the initiator cells of AML. LSCs have the capability of self-renewal, immortalization and multi-directional differentiation. LSCs are associated with the chemoresistance to different cytotoxic drugs, radiotherapy, primarily responsible for AML relapses, and poor prognoses. Therefore, targeted treatment of LSCs could control the regeneration of AML.[3,4]

It was known that intracellular reactive oxygen species (ROS) are important in regulating normal cellular processes, but abnormal ROS levels contribute to the development of various human diseases. Cancerous cells with an innately high level of intracellular ROS have accommodated their accelerated metabolism, which distinguishes the cancerous cells from normal cells.[5,6] However, LSCs possess low ROS level, which may be one of the important factors related to AML's drug resistance.[7,8]

Studies have demonstrated that $Fe_3O_4$ nanoparticles ($Fe_3O_4$ NPs), also called iron oxide nanoparticles (IONPs), are a member of the recently discovered nanozyme-like family. IONPs have the function of horseradish peroxidase (HRP) without any modification on the surface. For example, in acidic condition, IONPs can catalyze the reaction of hydrogen peroxide to generate hydroxyl radicals, which leads to an increase in ROS level.[9–12] The modulation of intracellular ROS level is crucial to cellular homeostasis because the different ROS levels can induce different biological responses.[13–15] In addition, engineered multiply functional IONPs have shown pronounced biological activities, including antibacterial action against different bacteria[16,17] and antitumor action against different tumors.[18–20]

In the present study, we developed nanozyme-like IONPs to evaluate its effects on LSCs ($CD34^+CD38^-$cells),[21–23] which were isolated from the KG1a cells, a human AML cell line, when the nanozyme-like IONPs were administered in combination with the chemotherapeutic drug Ara-C. Our study exhibited the regulation of ROS level in LSCs and provided evidence that the AML relapse might be controlled by a targeted inducing of LSC apoptosis.

# Materials and Methods

## Materials

### Cell Lines

Human AML cell lines KG1 and HL-60 were purchased from the Cell Institute of Chinese Academy of Sciences in Beijing, People's Republic of China. Human AML cell line KG1a was a generous gift from Prof. Haiyan Xu, Chinese Academy of Medical Sciences, Basic Medicine Institute, Beijing, China. Cells were grown in IMDM medium (Thermo Fisher Scientific, Waltham, MA, USA) supplemented with 10% Fetal Bovine Serum (FBS; Thermo Fisher Scientific), 2mM L-glutamine, and 100U/mL penicillin, 100μg/mL streptomycin at 37 °C in a humidified incubator containing 5% $CO_2$. All cell lines used in the study were approved by the ethics committee of Southeast University.

### Chemicals

All the chemicals and media components used in the present study were procured from Nuclear Industry Institute of Physical and Chemical Engineering (Shanghai, China), BD Biosciences (San Jose, CA, USA), and Sigma-Aldrich (St. Louis, MO, USA).

### Antibodies, Primers, and Compounds

Primary antibodies for gp91-phox (Rabbit anti Human polyclonal antibody, pAb), superoxide dismutase 1 (SOD1) (Rabbit anti Human polyclonal antibody, pAb), GAPDH (Rabbit anti Human monoclonal antibody, mAb), and HRP Secondary Goat anti Rabbit antibody were purchased from Proteintech Group, Inc. (Wuhan, China). CD34-FITC (Rabbit anti Human pAb) and CD38-APC (Rabbit anti Human pAb) were purchased from Biolegend (Way San Diego, CA, USA).

Gene specific quantitative real-time polymerase chain reaction (qRT-PCR) primers for GAPDH (Forward: 5′-CGGAGTCAACGGATTTGGTCGTAT-3′, Reverse: 5′-AGCCTTCTCCATGGTGGTGAAGAC-3′), CD38 (Fwd: 5′-GCTCAATGGATCCCGCA GTA-3′, Rvs:5′-GGATCC TGGCATAAGTCTCTGG-3′), DEP domain-containing mTOR-interacting protein (DEPTOR) (Fwd: 5′-GGTGC

GAGGAAGTAAGCCAT-3′, Rvs:5′-TTGAGCCCGTTGA CAGAGAC-3′), interferon-inducible transmembrane3 (IFITM3) (Fwd:5′-CATCGTCATCCCAGTGCTGAT-3′, Rvs: 5′-TGGAAGTTGGAG TACGTGGG-3′), were obtained from Gene and Technology (Shanghai, China).

$Fe_3O_4$ NPs (IONPs) were generously provided by Prof. Ning Gu, School of Biological Science and Medical Engineering, Southeast University, Nanjing, China. Ara-C was procured from Dalian Meilun Biotech CO., Ltd (DD-port (DIGITAL&DNA), China).

## Methods

### Preparation of AML $CD34^+CD38^-$Cells

The $CD34^+CD38^-$cells were isolated from the human AML cell line KG1a by magnetic activated cell sorting method (MACS; Miltenyi Biotec, Gladbach, Germany) following our previous studies.[24,25] We named $CD34^+CD38^-$cells for AML-SCs. This was accomplished through our subsequent analysis of the $CD34^+CD38^-$cells that shared the CSC characteristics.[26,27] To detect the purity of $CD34^+CD38^-$LSCs and expression of the CD45 in mice, the CD34 CD38, and CD 45 antibodies (eBioscience) were applied on a flow cytometry (FCM; BD Biosciences) according to the manufacturer's instructions and as described previously[28].

### Drug Dose Response Viability and Cell Proliferation Assays

To determine the cytotoxic effect of Ara-C on LSCs and non-LSCs, $2\times10^4$ LSCs or non-LSCs/well were plated into 96-well plates. Cells were treated with Ara-C in various drug concentrations (0, 0.0625, 0.25, 1, 4, and 16μM /well) in triplicate wells for 48h. After 48h of incubation, 10μL/well CCK8 assay Kit (Sigma-Aldrich Co., St. Louis, MO, USA) was added to the cells and further incubated for 4h. Microplate Reader (Bio-Rad Laboratories, Inc., Hercules, CA, USA) at optical density (OD) $_{450}$ was measured and OD value was recorded. The result was analyzed by Graph Pad software (Version: 5.0).[29] After the optimal drug concentration was selected, $2\times10^3$ LSCs and non-LSCs were plated into 96-well plates for the cell proliferation assay at 0h, 24h, 48h, 72h, 96h, and 120h, respectively. According to OD value, the cell proliferative activity was evaluated at 120h.

## Clonogenic Assay

$1\times10^6$ LSCs or Non-LSCs were treated with the different agents following our previous reports.[30,31] One hundred single-cell suspension cells were resuspended in 0.8mL IMDM medium containing 0.3% low melting temperature agarose (Promega, Fitchburg, MI, USA) and were plated in triplicate on 24-well plate over a base layer of 0.8 mL IMDM medium containing 0.6% low melting temperature agarose. The plate was incubated for 12–14 days until colonies were developed. Colony diameter larger than 75μm or colony cells more than 50 cells were then counted as 1 positive colony.

## Determination of Intracellular ROS Level

ROS generation was investigated as previously reported.[32,33] LSCs and Non-LSCs at the density of $1\times10^6$/mL medium were treated with phosphate-buffered saline (PBS), Ara-C (0.4μM), IONPs (150 μg/mL), and Ara-C (0.4μM)+IONPs (150μg/mL) incubated at 37 °C for 24 h. Twenty-five mins prior to the end of incubation, 5 μM chloromethyl dihydro 2′ 7' dichloro-fluorescein diacetate (DCFH-DA, Njjcbio, China) was added to cells at 37 °C. At the completion of incubation, samples were placed on ice. The production of ROS in LSCs and Non-LSCs was measured by fluorescence intensity following dichlorofluorescein staining using FCM (BD Biosciences).

## Apoptosis Measurements

The apoptotic rate was assessed by using Annexin V- APC/PI Apoptosis Detection Kit (Fcmacs, China). Generally, LSCs and Non-LSCs were respectively plated in six-well plates ($2\times10^6$ cells/well) and treated with various agents for 24 h. Subsequently, cells were washed with PBS and resuspended in binding buffer. Aliquots (100 μL) of $10^6$ cells/mL were incubated with 5 μL of annexin V-APC and 10 μL propidium iodide (PI) for 15 min in the dark at room temperature, prior to the evaluation of cell apoptosis by FCM analysis[34].

## qRT-PCR

qRT-PCR was performed as previously reported.[35,36] Briefly, RNA was extracted from each sample by using a Qiagen RNeasy Kit (Qiagen, Valencia, CA, USA). Concentration of the extracted RNA was measured with Nano Drop ND-1000 Spectrophotometer (Nano Drop Technologies, Thermo Fisher Scientific). One microgram of total RNA per sample was subjected to cDNA synthesis using the Superscript III Reverse Transcriptase (Invitrogen, Thermo Fisher Scientific). The mRNA levels of the genes of interest were expressed as the ratio of each gene of interest to GAPDH mRNA for each sample. The fold change in gene expression was calculated with the

$2^{-\Delta\Delta Ct}$ method and the presented data were normalized to the mesothelium values.

## Western Blots

Cells were plated at $1\times10^6$ cells/well in 6 well plates and allowed to grow for 24 h and treated with various agents for another 24 h after the incubation. Treated cells were washed in PBS. Gel electrophoresis was performed on 10-well 1.5 mm NuPAGE 12% Bis-Tris gels (Thermo Fisher Scientific). Samples were then transferred to Invitrolon PVDF transfer membranes (Invitrogen, Thermo Fisher Scientific) and blocked overnight at 4 °C or 1 h at room temperature in blocking buffer consisting of 1× TBS (Quality Biological) with 0.1% Tween® 20 (Thermo Fisher Scientific) and 5% dehydrated milk. Primary antibodies were used at concentration of 1:1000 except the GAPDH control that was used at concentration of 1:2000. The membrane was rinsed for 5 min with an antibody wash solution for 3 times. The secondary antibody concentration used was at a 1:5000 dilution for 1 h at room temperature, and the following steps were performed according to the kit's protocol.[37,38]

## In vivo Experiment

The animal experiments were carried out in agreement with the Guidelines of the Animal Research Ethics Board of Southeast University. Full details of the study approval can be found in the approval ID: 20080925. The Animal Research Ethics Board of Southeast University approved the present animal studies and the approval number was 20190128. All the mice were maintained in a pathogen-free facility that has a 12-hour light/dark cycle and relative humidity ranged from 50% to 60% at 24°C. The released cells from each group were transplanted into the nonobese diabetic/severe combined immune deficiency (NOD/SCID) mice ($5\times10^5$ LSCs or PBS) through caudal vein inoculation at 5 weeks of age with 16.88 ± 0.51 grams in weight, which were purchased from Beijing Weitong Lihua Experimental Animal Technology Co., Ltd., China (Animal certificate number: SCXK (Beijing) 2016-0006). Fifteen days after injection, the mice transplanted with Non-LSCs or LSCs were randomly divided into eight groups of equal size (3 mice), including four Non-LSC groups and four LSC groups. AML model group (treated with PBS 200μL), IONPs group (treated with 10 mg/kg IONPs), Ara-C group (treated with 50mg/kg Ara-C), and Ara-C-IONPs group (treated with 50mg/kg Ara-C+10 mg/kg IONPs). To assess the antitumor effects of various agents, 200μL of each agent were intravenously injected into AML-bearing mice once every three days a total of five times. To test leukocyte classification, the blood routine samples were collected from the venous plexus of eye sockets in mice. The peripheral blood leukocyte classification and hemoglobin (HGB) were tested On Day 0, Day 10, Day 20, and Day 30, respectively. Mice were sacrificed 33 days later and mouse tissues were collected and histological examination was performed. The animal experiment was repeated twice.[39,40]

## Statistical Analysis

The data were plotted as mean ± SD and analyzed for statistical significance by two-tailed paired Student's *t* test or repeated measures analysis of variance (ANOVA). *P* values less than 0.05 were considered statistically significant. Analyses were performed with the SPSS 19.0 software package.

# Results and Discussion

## LSCs Were Isolated and Identified in vitro

AML is a hematopoietic system disease that tends to relapse due to the existence of LSCs. It is well known that LSCs are responsible for chemoresistance and this is the primary cause for the clinical failure in elimination of AML cells[5]. In this study, to evaluate the effects of nanozyme-like IONPs and Ara-C on LSCs from AML cell line KG1a, we first analyzed the percentage of $CD34^+CD38^-$ cells in human AML cell lines of HL-60, KG1 and KG1a since the $CD34^+CD38^-$ phenotype cells are contributed to LSCs.[21,22] In Figure 1A, the results analyzed by FCM showed that a very small fraction of $CD34^+CD38^-$cells were found in the HL-60 cells (0.912%) and the KG1 cells (7.30%), but 32.9% of $CD34^+CD38^-$cells were found in the KG1a cells. Based on these findings, we used the KG1a cells to isolate the $CD34^+CD38^-$cells. Following a standard protocol and our previous reports,[24,25] we isolated the $CD34^+CD38^-$cells by MSAC. The percentage of $CD34^+CD38^-$ phenotype cells was found to be around 94.3% (Figure 1A). This result suggested that the purity of the $CD34^+CD38^-$ cells isolated by MSAC was acceptable for use in subsequent study.

To identify the characteristics of $CD34^+CD38^-$cells, we analyzed the resistance to chemotherapeutic drug in $CD34^+CD38^-$LSCs incubated with Ara-C in varying concentrations using the CCK8 assay. Figure 1B illustrated the cellular viability of LSCs and Non-LSCs was decreased as

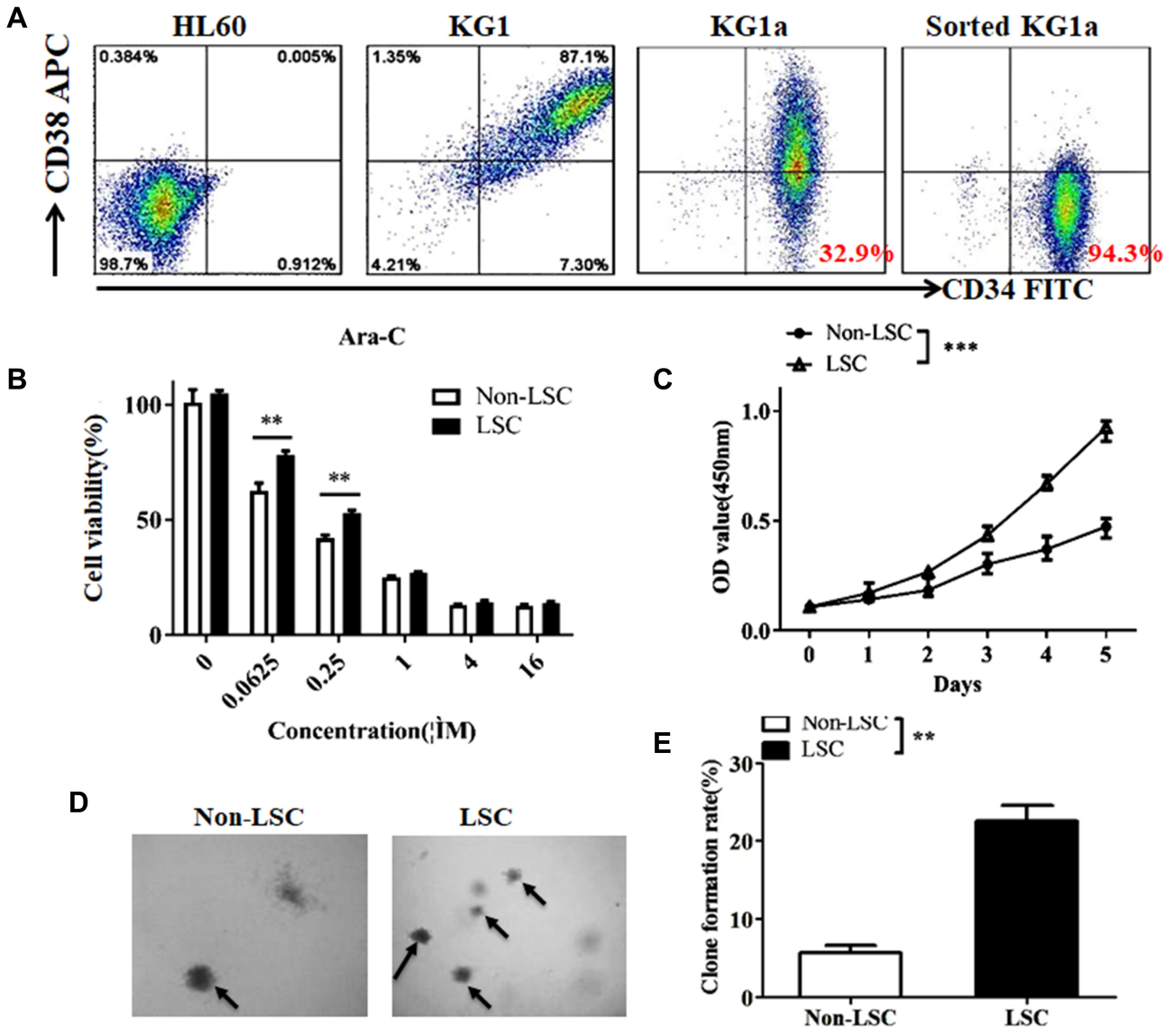


**Figure 1** Isolation and identification of LSCs. (**A**) FCM analysis of $CD34^+CD38^-$cells in HL-60 cells (0.912%), KG1 cells (7.30%), and KG1a cells (32.9%). Isolation of $CD34^+CD38^-$cells by magnetic activated cell sorting method from KG1a cell line and the purity of $CD34^+CD38^-$cells (94.3%) was identified by FCM. (**B**) Cellular viability assay for LSCs and Non-LSCs incubated with various concentration of Ara-C (μM). (**C**) Cell proliferation assay for LSCs and Non-LSCs in vitro. (**D**) Clone assay for LSCs and Non-LSCs in the soft agar media. The black arrows represent the positive clones. (**E**) Statistical analysis of clone formation rate. $^{**}p$ <0.01 and $^{***}p$<0.001 were calculated by *t* test, referring to the statistically significant difference as compared to respective group.

Ara-C concentration was increased step by step. It was found that Ara-C was at concentration of 0.0625 μM and the cellular viability of Non-LSCs was significantly reduced compared with that of LSCs (79% vs 61%, $P$<0.01). However, the cellular viability did not show remarkable difference between LSCs and Non-LSCs when the Ara-C concentration went over 1μM, which indicated the significant increase in the cytotoxicity conferred by Ara-C. Therefore, we applied the Ara-C at concentration of 0.4 μM in our subsequent experiments. Figure 1C shows that the proliferative ability of LSCs was gradually increasing compared with that of Non-LSCs in the IMDM medium, especially in the 5 day-culture, and the difference in change was statistically significant ($p$ < 0. 005).

The clone formation ability in the soft agar is used to measure the ability of cells to cross tissue barriers and cell invasion. The cloning efficiency is correlated positively with the disease stage of multiple myeloma, plasma cell leukemia or advanced multiple myeloma.[30,41] For this reason, we assessed the clone formation ability of LSCs in soft agar medium. Figure 1D shows that LSCs formed more clones than that of Non-LSCs and the colony formation rate in the soft agar media was around 21% for the LSCs and 7% for the Non-LSCs when measured 14 days

after the incubation. The difference was statistically significant ($p<0.01$) as shown in Figure 1E. Overall, the data analysis showed that the $CD34^+CD38^-$cells isolated from the KG1a cells possessed the LSC's characteristics, such as more resistant to chemotherapeutic drug Ara-C and stronger clone formation ability than those of Non-LSCs. Therefore, the $CD34^+CD38^-$cells were identified as LSCs. The isolated LSCs were cultured in the IMDM medium in 4h for the subsequent experiments to avoid LSC differentiation.

## IONPs Combined with Ara-C Increased LSC Apoptosis via Enhancing ROS Level

To assess the effect of IONPs on LSCs, we first observed the cytotoxicity of IONPs on the KG1a cells with the 50% inhibiting concentration ($IC_{50}$) assay in this study. Figure 2A indicates that no cytotoxicity to KG1a cells was present when IONPs was at concentration of 20 μg/mL or 60μg/mL, but when the concentration was over 180μg/mL, the apoptosis level in the KG1a cells was significantly increased compared with that at concentration of 20 μg/mL or 60μg/mL (Figure 2A and B). In another preliminary experiment, $IC_{50}$ of IONPs in the KG1a cells was found to be around 145.2± 7.6 μg/mL (data not shown here). Therefore, IONPs was used at concentration of 150 μg/mL in the subsequent experiments. Figure 2C shows no significant differences were found in apoptosis levels (Control) between the LSCs and the Non-LSCs when incubated with IONPs at concentration of the 150 μg/mL. On the other hand, the apoptosis level was increased in Non-LSCs compared to LSCs incubated with Ara-C at concentration of 0.4μM, especially in Ara-C (0.4μM) plus IONPs (150μg/mL), and the difference statistically significant (Figure 2D). It is known that caspase-8 and caspase-9 are activated via the death receptor and mitochondrial signaling pathways during apoptosis,

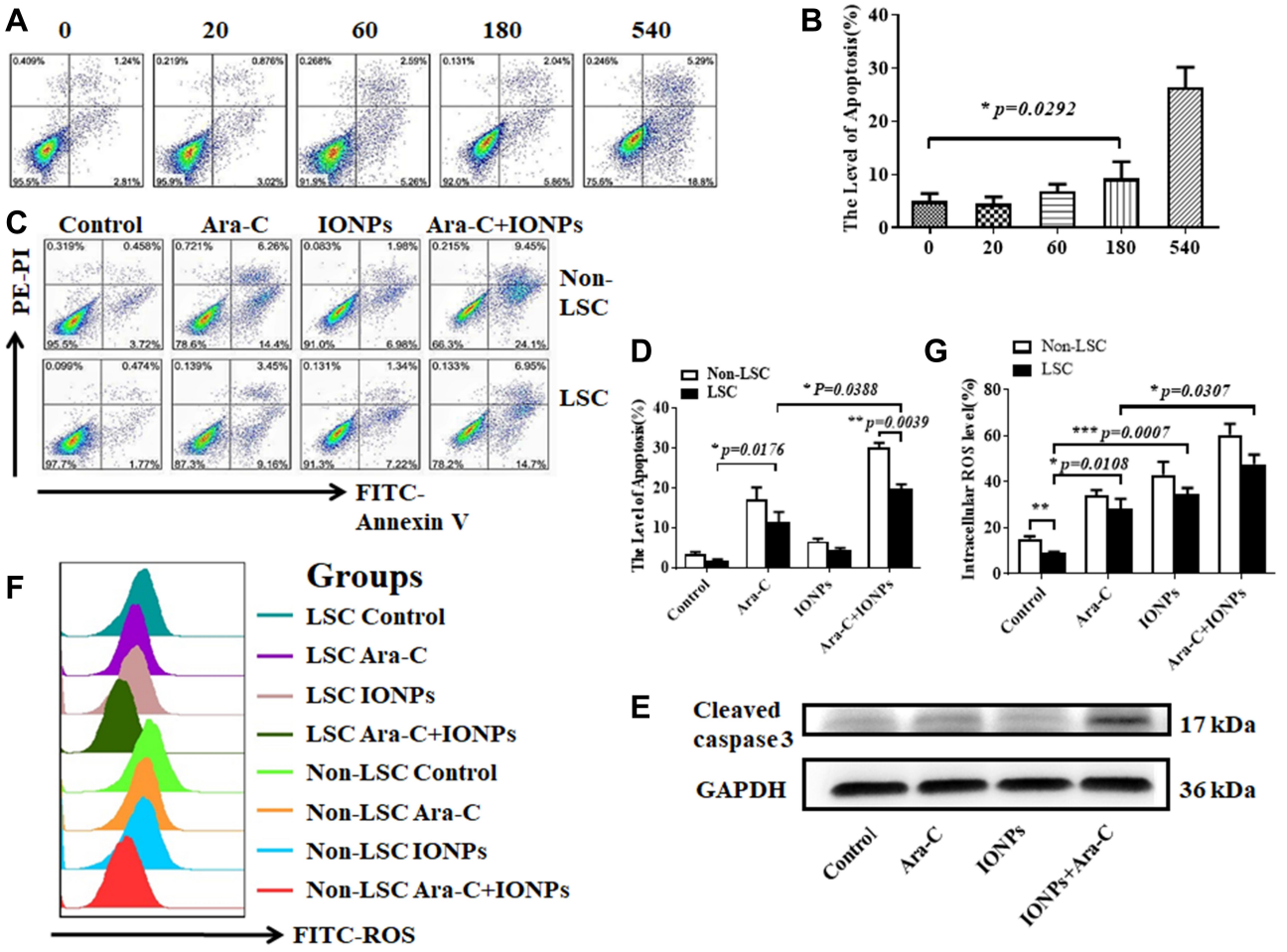


**Figure 2** FCM analysis of levels of apoptosis and ROS in LSCs and Non-LSCs treated with different agents. (**A**) $IC_{50}$ assay for KG1a cells analyzed by FCM and the cytotoxicity of IONPs to KG1a cells incubated with various concentration of IONPs (μg/mL). (**B**) Statistical analysis of the apoptosis rate. (**C**) FCM analysis of apoptosis rates of LSCs and Non-LSCs incubated with various agents. (**D**) Statistical analysis of apoptosis rates. (**E**) The cleaved caspase-3 expression analyzed by Western blot. (**F**) FCM analysis of ROS levels in LSCs and Non-LSCs treated with different agents. (**G**) Statistical analysis of ROS level in LSCs and Non-LSCs. *$p$ <0.05, **$p$ <0.01 and ***$p$ < 0.001 were calculated by $t$ test, referring to the statistically significant difference as compared to respective group.

whereas caspase-3 is a common effector of both signaling pathways.[42] We speculate that IONPs combined with Ara-C might induce the LSC apoptosis via both caspase-dependent receptor and mitochondrial apoptotic pathways. Therefore, we detected the important biomarker for apoptosis, a cleaved caspase-3, by Western blot. The high expression of cleaved caspase-3 further confirmed the cell apoptosis effect induced by IONPs plus Ara-C (Figure 2E).

Recent advances in research demonstrate that high ROS content in cancer cells makes them more susceptible to oxidative stress to induce cell death, and this evidence can be exploited for targeted selective AML treatment by aiming at modulation of ROS level in AML cells.[5,8] To this end, we reasoned that the increased apoptosis level in LSCs treated with IONPs combined with Ara-C may be associated with the elevated ROS level. Since IONPs can catalyze the reaction of hydrogen peroxide to lead to elevated ROS levels in cancerous cells, we next analyzed the ROS level in LSCs. Interestingly, the ROS levels in both LSCs and Non-LSCs were significantly increased when cultured with IONPs compared to the control without any agents. Moreover, the ROS level in the cells treated with IONPs was higher than that of the cells treated with Ara-C, especially in the cells treated with IONPs combined with Ara-C. The differences were statistically significant ($p < 0.0108$, $p < 0.0007$, and $p < 0.0307$) (Figure 2F and G). It has been reported that one of stem cell's features is their low ROS level.[7,8] Our data was consistent with the reports and showed that the ROS level was lower in LSCs than Non-LSCs (Figure 2F). Our findings from the data let us conclude that the IONPs combined with Ara-C increased the apoptosis in LSCs and Non-LSCs through enhancing the ROS levels. This findings also agreed with previous studies that the $Fe_3O_4$ composite can be used as an effective inhibitor of antibiotic resistance in medicine, including nanoparticles carrying chemotherapeutic agents used in cancer treatment; our result suggested that the good efficacy might be due to improving the ROS level.[43–45] Thus, we believed that the combination of a conventional cancer drug Ara-C and the IONPs to target upregulation of ROS would be a better approach than using chemotherapeutic agents alone to improve drug-sensitivity for treating AML patients.

## IONPs Plus Ara-C Improved gp91-phox but Decreased SOD1 Expression in LSCs

The intracellular ROS level is associated with a complex interplay in the modulation of ROS production, such as autophagy and apoptosis in response to various molecular expression.[13,46] It is known that gp91-phox may improve ROS level, but SOD1, an important antioxidant enzyme, could convert ROS in cancerous cells to hypochlorous acid and subsequent singlet oxygen species that might mediate the inhibition of cancerous cell proliferation. Nevertheless, both gp91-phox and SOD1 are related with the regulation of ROS level and oxidative stress.[47–49] Therefore, we further detected the expression levels of gp91-phox and SOD1 by Western blot. Figure 3A shows that the expression of gp91-phox was markedly increased in the Non-LSCs treated with IONPs, particularly in the Non-LSCs treated with IONPs plus Ara-C; the difference between the IONPs and IONPs plus Ara-C was statistically significant. On the other hand, the gp91-phox expression did not reveal any significant change in Non-LSCs treated with Ara-C only (Figure 3C). According to this result, we reasoned that Ara-C could have forcefully inhibited the synthesis of DNA polymerase, as well as DNA polymerization and synthesis, but the action of Ara-C was not involved in impacting on the expression of gp91-phox, a component of nicotinamide-adenine dinucleotide phosphate (NADPH) oxidase that serves as an electron carrier in a number of reactions, when being alternately oxidized (NADP+) and reduced NADPH. Figure 3A and C also showed that the expression of gp91-phox was significantly up-regulated in Non-LSCs and LSCs compared to the control cells without adding any agent, especially in Non-LSCs in the presence of IONPs plus Ara-C. In contrast, the expression of SOD1 was markedly down regulated in LSCs treated with IONPs, Ara-C, and IONPs combined with Ara-C, respectively, compared with the control cells; however, the SOD1 expression did not chang in Non-LSCs when incubated with IONPs, Ara-C, and IONPs combined with Ara-C, respectively (Figure 3B and D). Collectively, these results demonstrated that IONPs and IONPs plus Ara-C increased the gp91-phox expression but decreased the SOD1 expression in LSCs, which might increase the ROS level to induce the LSC apoptosis.

In addition, we simultaneously detected the expression of LSC-related genes including CD38, DEPTOR (pleckstrin domain-containing mTOR-interacting protein), which is an inhibitor of the mTOR kinase that controls cell growth,[50] and IFITM3 (interferon-induced transmembrane protein 3), which is an antiviral factor that inhibits viruses to enter host cells through acidic endosomes[51] by using RT-qPCR. As expected, the expression levels of CD38 and DEPTOR were down regulated in LSCs when treated with IONPs, Ara-C, and IONPs combined with Ara-C, respectively,

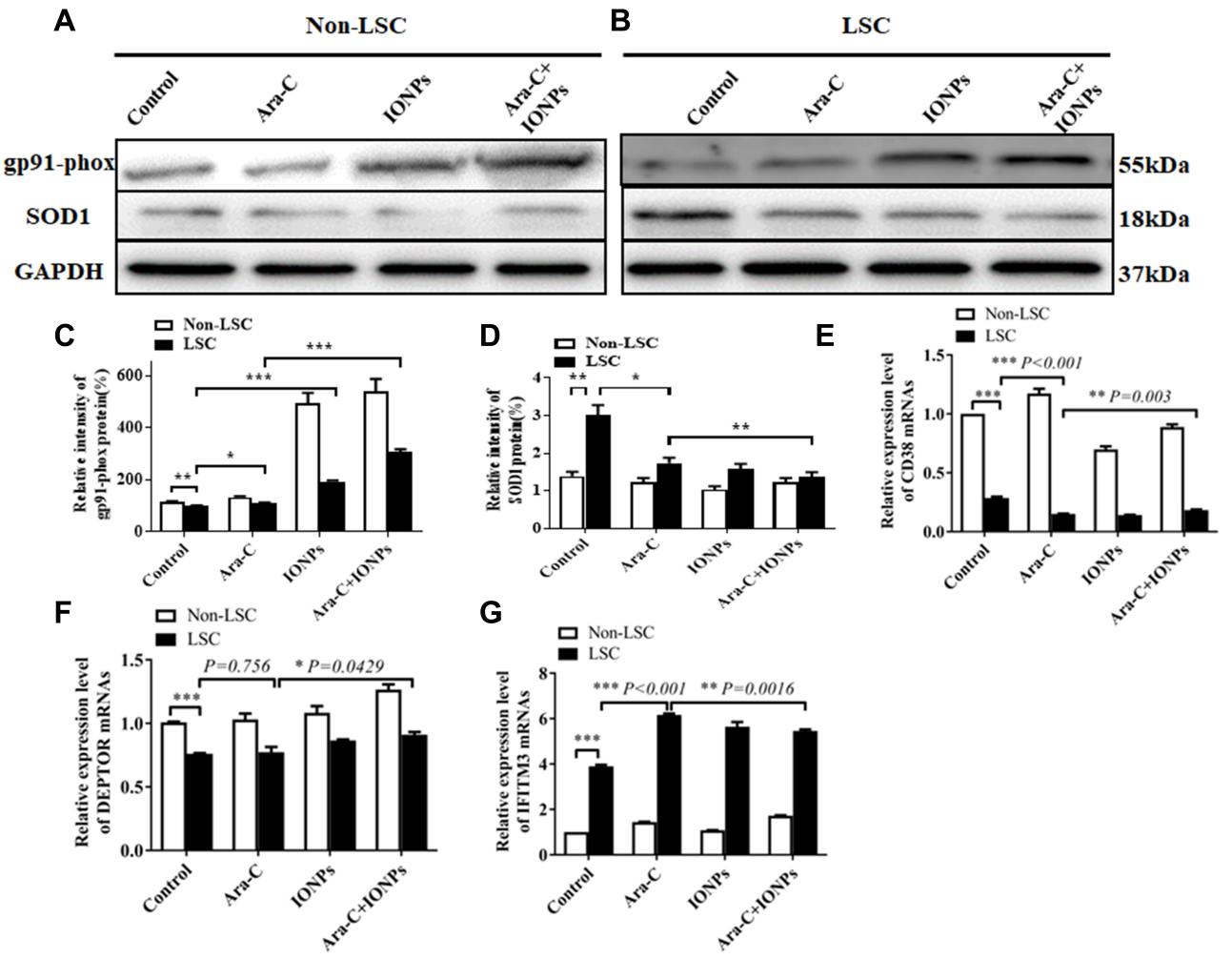


**Figure 3** Analysis of the expression levels of gp91-phox and SOD1. (**A** and **B**) The expression levels of gp91-phox and SOD1 analyzed by Western Blot in LSCs and Non-LSCs treated with different agents. (**C**–**G**) Semi-quantification of the expression levels of gp91-phox, SOD1, CD38, DEPTOR, and IFITM3 detected by RT-qPCR in LSCs and Non-LSCs treated with different agents. *$p$ <0.05, **$p$ <0.01 and ***$p$ < 0.001 were calculated by $t$ test, referring to the statistically significant difference as compared to respective group.

compared with the Non-LSCs. In contrast, the IFITM3 expression was upregulated in LSCs when incubated with IONPs, Ara-C, and IONPs plus Ara-C compared to Non-LSCs, respectively (Figure 3E and F); but there was no significant change in Non-LSCs in the presence of IONPs, Ara-C, and IONPs plus Ara-C, respectively, compared with the LSCs (Figure 3G). More recently, emerging data have revealed that overexpression of IFITM3 has been observed in glioma, head and neck cancer, lung cancer, and breast cancer.[6,52] Therefore, LSCs have high expression of IFITM3 and low expressions of CD38 and DEPTOR, which are involved in the stem-like characteristics of LSCs. Our current preliminary findings suggested that the IONPs combined with Ara-C could impact the expression levels of CD38, DEPTOR, and IFITM3 in LSCs, which in turn might further impact LSC's characteristics, resulting in changing the resistance to chemotherapeutic drugs. Based on the results, we think that additional studies aimed at the intricacies of IFITM3 overexpression and how this expression can be inhibited may be instrumental for the design of novel targeted strategy to control AML.

## Establishment of a AML Xenograft Model

To evaluate the effects of IONPs combined with Ara-C on LSCs in vivo, we first established an AML xenograft model. NOD/SCID mice were injected with $5\times10^5$ $CD34^+CD38^-$ cells or PBS through tail veins. Twenty days after the injection, AML-bearing mice were in low spirits, and had less movement. The body weights and hemoglobins (HGB) level were remarkably reduced but the peripheral blood white cell (WBC) counts were markedly increased compared with the control mice injected with PBS. The spleens

of the AML-bearing mice were turgid swelling, and the spleen index was increased compared with the control mice; the differences were statistically significant (Figure 4A–E). The smears of the blood samples revealed abnormal blood cells in cell morphology, indicating round or ellipse shapes, a macro-nucleus and hypo-cytoplasm. The smears of the bone marrow samples stained by Wright-giemsa staining indicated the archaeocyte cells or juvenile cells, which exhibited morpho-irregularity, nuclear chromatin increase, and disproportion of nucleus and cytoplasm. The ratio of juvenile cells was markedly increased in the AML-bearing mice compared to control mice (Figure 4F and G). These results suggested that the AML xenograft mouse model was successfully established, and that the model mice shared many pathological characteristics with those of AML and was available for investigating treatment of AML diseases.

## Treatment of AML-Bearing Mice Using IONPs Combined with Ara-C

Having established the AML xenograft mouse model we evaluated the therapeutic effects of nanozyme-like IONPs combined with Ara-C (combination) on AML-driven xenograft progression in NOD/SCID mice by injection of Non-LSCs or LSCs. Fifteen days after injection, the mice were treated once every three days with PBS, IONPs, Ara-C and the combination, respectively, in total of five times. The demonstrated strong therapeutic activity of the treatment with various agents was apparently associated with the therapeutic efficacy

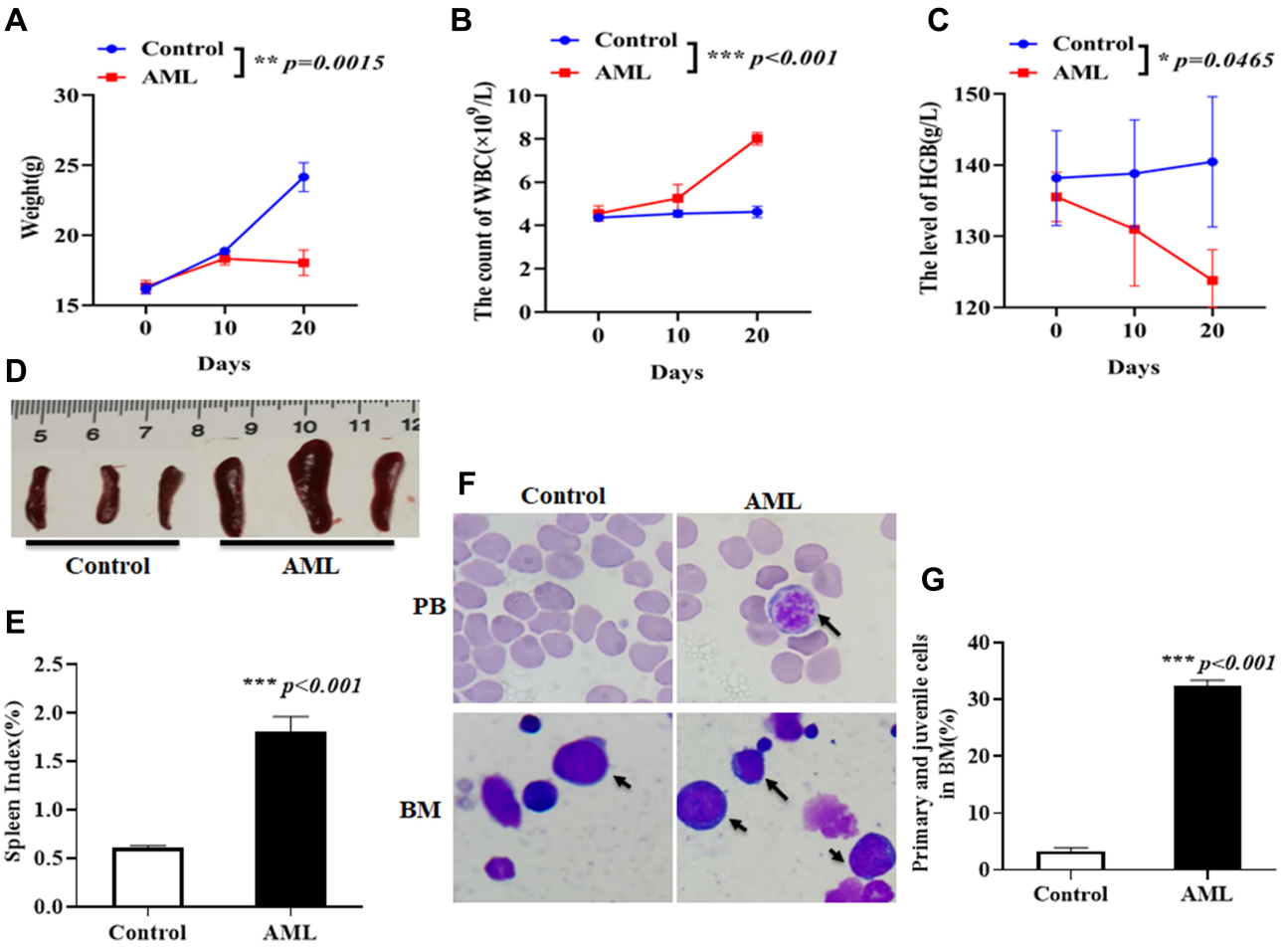


**Figure 4** Assessment of AML xenograft model in NOD/SCID mice. (**A**) Weight of mouse body weights once every 10 days in mice injected with $5\times10^5$ $CD34^+CD38^-$AML cells or PBS through tail veins. (**B**) WBC counts of peripheral blood once every 10 days in mice injected with $5\times10^5$ $CD34^+CD38^-$AML cells or PBS. (**C**) HGB level of peripheral blood once every 10 days in mice injected with $5\times10^5$ $CD34^+CD38^-$ AML cells or PBS. (**D**) Representative images of the size of spleens taken from the mice injected with $5\times10^5$ $CD34^+CD38^-$AML cells or PBS 30 days later. (**E**) The statistical analysis of spleen index in AML xenograft mice and control mice. (**F**) Representative images of AML cell shape (Wright-giemsa staining) on the smears of peripheral blood (PB, top, arrow, magnification × 1000) and juvenile cell shape (Wright-giemsa staining) on the smears of bone morrow (BM, bottom, arrow, magnification × 1000) in AML xenograft mice and control mice. (**G**) Statistical analysis of juvenile cell percentage in BM. *$p$ <0.05, **$p$ <0.01 and ***$p$ < 0.001 were calculated by $t$ test, referring to the statistically significant difference as compared to respective group.

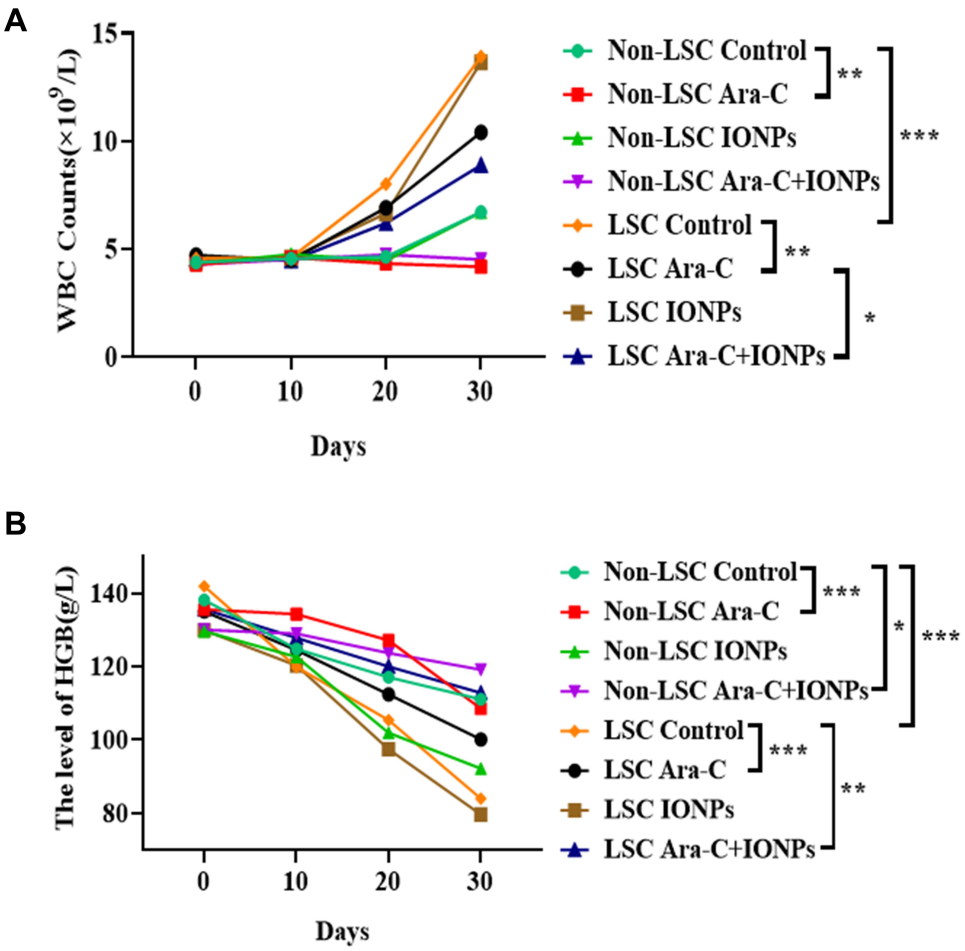


**Figure 5** Detection of WBC counts and HGB level in AML xenograft model after treated with different agents. (**A**) Dynamic state detection of WBC counts in AML bearing mice injected with Non-LSCs or LSCs after treated with different agents. (**B**) Dynamic state detection of HGB level in AML bearing mice injected with Non-LSCs or LSCs after treated with different agents. All the data represent as mean ± S.D. (n = 6); *$P < 0.05$, ** $P < 0.01$ and *** $P < 0.001$ were calculated by *t* test, referring to the statistically significant difference as compared to respective group.

to reduce abnormal WBC counts in the peripheral blood. As shown in Figure 5A, the highest WBC counts were found in the model mice transplanted with LSCs and treated with PBS. Similarly, the mice transplanted with LSCs were treated with IONPs alone also showed high counts of WBC; whereas the lowest WBC counts were found in the group of mice transplanted with Non-LSCs and treated with Ara-C only. Analogously, the mice injected with Non-LSCs were treated with the combination also showed low WBC counts; the differences were statistically significant (Figure 5A). In contrast, the highest level of HGB was found in the mice transplanted with Non-LSCs and treated with the combination. Moreover, the mice transplanted with LSCs and treated with the combination also showed high level of HGB. However, the lowest level of HGB was found in the group of mice transplanted with LSCs and treated with IONPs alone. Analogously, the mice transplanted with LSCs and treated with the PBS also showed low level of HGB, which were statistically significant (Figure 5B).

The morphous of AML cells in the AML bearing mice treated with various agents were further assessed by histological morphology. Figure 6B shows the AML cell morphous, as determined by Wright-giemsa staining, on the smears of blood samples that were collected from the LSC-transplanted mice treated with various agents. However, no AML cells were observed on the smears of the blood samples collected from the Non-LSC-transplanted mice treated with various agents (Figure 6A). The result suggested that Non-LSCs had hardly any growth under the selected pressure of various agents. Our data from the SCID mice transplanted with Non-LSCs agreed considerably with a previous report that the marrow implants from six patients in the chronic phase of CML showed infrequent and limited

myeloid growth in the mice.[40] Notably, on the smears of the bone marrow samples (Figure 6C and D), the percentage of primitive and immature cells was significantly increased in the mice transplanted with LSCs compared with the mice transplanted with Non-LSCs, particularly in the mice treated with IONPs alone. However, there were no significant differences between the combination and the Ara-C groups (Figure 6E).

The in vivo animal experiment results suggested that the IONPs seemed to have no active effect on the AML bearing mice. We analyzed that IONPs had no specific target destination and hardly entered the bone marrow to penetrate AML cells in the complicated internal milieu in vivo, and did not increase ROS level to induce AML cell apoptosis. On the other hand, the ROS-inducing cytotoxic drug Ara-C could minimize the adverse effects on normal cells by acting as antioxidants without interfering with their cytotoxic effects on AML cells as pro-oxidants.[6] Therefore, Ara-C exerted active effects on the AML bearing mice by decreasing abnormal WBC counts and increasing HGB level, particularly in the mice treated with combination.

To further evaluate the therapeutic effect of the combination by evaluating the tumor burden in vivo, we detected the KG-1a cells express human CD45 molecule by FCM. From the data shown in Figure 6F, we found that the $CD45^+$cells of bone marrow cell populations in mice treated with PBS was accounting for ~3.03%, whereas in mice treated with the combination, the $CD45^+$ cell population was only accounting for ~ 0.98%, and the $CD45^+$ cell population was around 1.20% for the Ara-C treated mice and 1.71% for the IONPs treated mice, suggesting reduced tumor burden in vivo after treated by various agents, especially in the combination treated mice.

In addition, we evaluated whether the combination could give rise to toxic damage to major organs, pathological examinations were used to assess the changes of liver and

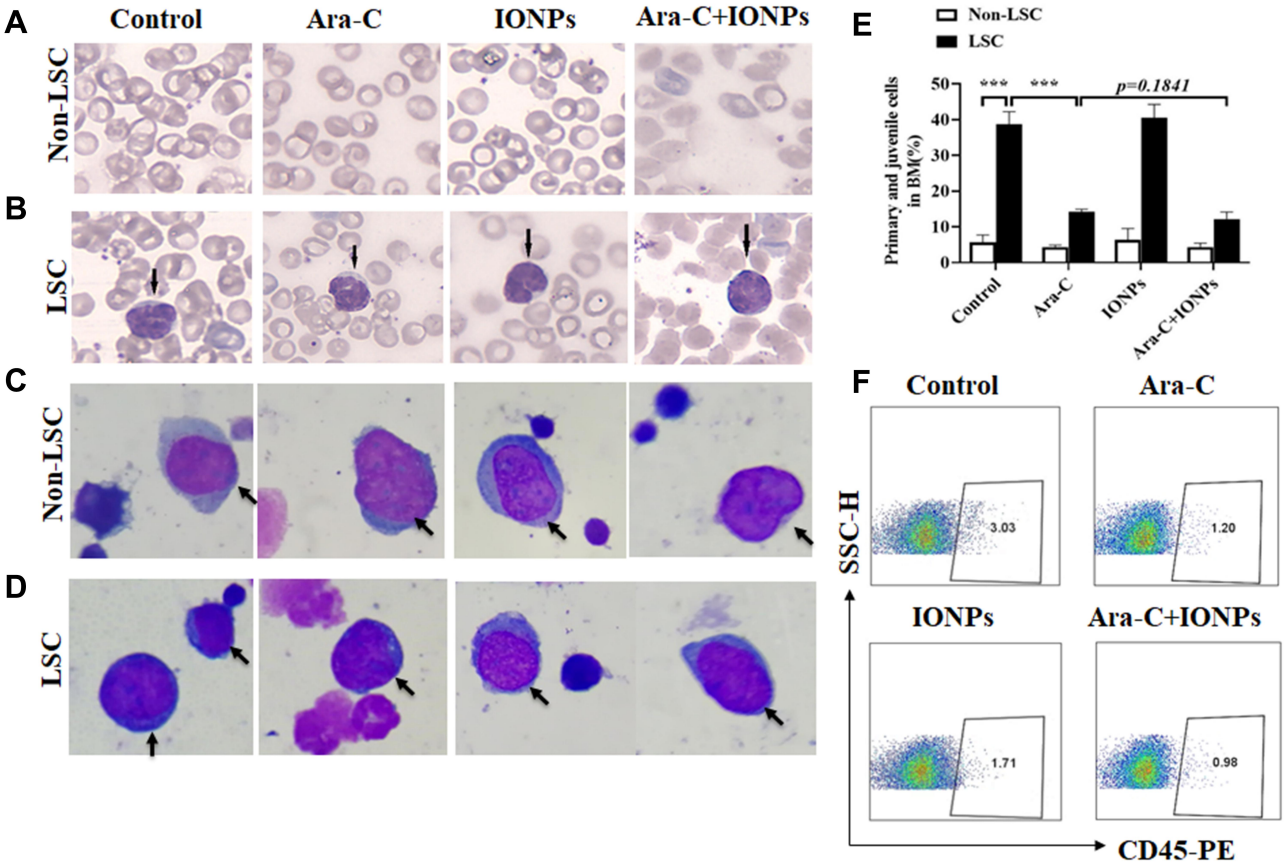


**Figure 6** Analysis of therapeutic effects of different agents on AML-bearing mice. (**A** and **B**) Representative images of blood cell shape (**A**) and AML cell shape (**B**) (Wright-giemsa staining, arrow, magnification × 400) on the smears of peripheral blood samples collected from the mice injected with LSCs after treated with different agents. (**C** and **D**) Representative images of juvenile cell shape (Wright-giemsa staining, arrow, magnification × 1000) on the smears of bone morrow (BM) in Non-LSCs (**C**) and in LSCs (**D**) xenograft mice after treated with different agents. (**E**) Statistical analysis of juvenile cell percentage of BM in mice after treated with different agents. (**F**) FCM analysis of the $CD45^+$cells of bone marrow cell populations in mice treated with various agents. ***$p<0.001$ was calculated by *t* test, referring to the statistically significant difference as compared to respective group.

kidney by H&E staining. The results showed that the morphology of liver and kidney tissue were all normal, indicating that the combination did not cause major adverse events associated with therapy (data not shown here).

Based on these results, we may conclude that the established AML xenograft mouse model could be used to evaluate in vivo efficacy of the AML-therapy with the different agents. The combination of IONPs and Ara-C exerted the therapeutic efficacy in decreasing AML burden and improving survival in the mice engrafted with LSCs.

## Conclusion

We focused on the $CD34^{+}CD38^{-}$cells in this study because the cells shared LSC's characteristics, which were determined by the assays of resistance to chemotherapeutic drug Ara-C, the cellular proliferation, and clone formation. Importantly, the in vitro and in vivo results demonstrate that the combination of the nanozyme-like IONPs and Ara-C exhibited high efficiency for the AML-therapy. The combination revealed an increase in the levels of apoptosis and ROS in LSCs by improving the p91-phox expression and decreasing the SOD1 expression. Our data also demonstrates that the SCID mouse is a reproducible system for the propagation of AML via tail veins implantation of LSCs. We believe that this initial research of ours may provide a viable alternative to making the combination of IONPs and Ara-C capable of treating LSCs without external energy activation, which may act as a potent trigger of the ROS-mediated LSC apoptosis for reducing AML relapses.

## Acknowledgments

Authors are thankful to Prof. Haiyan Xu, Chinese Academy of Medical Sciences, Basic Medicine Institute for providing KG1a cell line; Prof. Ning Gu, School of Biological Science and Medical Engineering, Southeast University for providing $Fe_3O_4$ NPs to complete this work. Authors are also thankful to Dr. Zeye Shao, Department of Clinical Laboratory, Zhongda Hospital Affiliated to Southeast University, Nanjing 210009, China, for identifying cell morphology on the smears of the blood and bone marrow samples.

## Funding

The study has been supported by the National Key Research and Development Program of China (2017YFA0205502), and partly supported by the National Natural Science Foundation of China (No. 81572887), as well as the Postgraduate Research & Practice Innovation Program of Jiangsu Province (KYCX18_0165).

## Disclosure

The authors declare no conflicts of interest in this work.

## References

1. Singh A, Myklebust NN, Furevik SMV, et al. Immunoliposomes in acute myeloid leukaemia therapy: an overview of possible targets and obstacles. *Curr Med Chem*. 2019;26(28):5278–5292. doi:10.2174/0929867326666190517114450
2. Thol F, Ganser A. Treatment of relapsed acute myeloid leukemia. *Curr Treat Options Oncol*. 2020;21(8):66. doi:10.1007/s11864-020-00765-5
3. Guo J, Russell EG, Darcy R, et al. Antibody-targeted cyclodextrin-based nanoparticles for siRNA delivery in the treatment of acute myeloid leukemia: physicochemical characteristics, in vitro mechanistic studies, and ex vivo patient derived therapeutic efficacy. *Mol Pharm*. 2017;14(3):940–952. doi:10.1021/acs.molpharmaceut.6b01150
4. Mandal T, Beck M, Kirsten N, Lindén M, Buske C. Targeting murine leukemic stem cells by antibody functionalized mesoporous silica nanoparticles. *Sci Rep*. 2018;8(1):989. doi:10.1038/s41598-017-18932-4
5. Nogueira V, Hay N. Molecular pathways: reactive oxygen species homeostasis in cancer cells and implications for cancer therapy. *Clin Cancer Res*. 2013;19(16):4309–4314. doi:10.1158/1078-0432.CCR-12-1424
6. Shin J, Song M-H, Jae-Wook O, Keum Y-S, Saini RK. Pro-oxidant actions of carotenoids in triggering apoptosis of cancer cells: a review of emerging evidence. *Antioxidants (Basel)*. 2020;9(6):E532. doi:10.3390/antiox9060532
7. Xiaotian X, Zhang X, Wei C, et al. Targeting SLC7A11 specifically suppresses the progression of colorectal cancer stem cells via inducing ferroptosis. *Eur J Pharm Sci*. 2020;152:105450. doi:10.1016/j.ejps.2020.105450
8. Han J, Won M, Kim JH, et al. Cancer stem cell-targeted bio-imaging and chemotherapeutic perspective. *Chem Soc Rev*. 2020;49(22):7856–7878. doi:10.1039/d0cs00379d
9. Srikanth Vallabani NV, Karakoti AS, Singh S. ATP-mediated intrinsic peroxidase-like activity of $Fe_3O_4$-based nanozyme: one step detection of blood glucose at physiological pH. *Colloids Surf B Biointerfaces*. 2017;153:52–60. doi:10.1016/j.colsurfb.2017.02.004
10. Gao L, Zhuang J, Nie L, et al. Intrinsic peroxidase-like activity of ferromagnetic nanoparticles. *Nat Nanotechnol*. 2007;2(9):577–583. doi:10.1038/nnano.2007.260
11. Fan K, Wang H, Xi J, et al. Optimization of Fe3O4 nanozyme activity via single amino acid modification mimicking an enzyme active site. *Chem Commun (Camb)*. 2016;53(2):424–427. doi:10.1039/C6CC08542C
12. Fan K, Cao C, Pan Y, et al. Magnetoferritin nanoparticles for targeting and visualizing tumour tissues. *Nat Nanotechnol*. 2012;7(7):459–464. doi:10.1038/nnano.2012.90
13. Cairns RA, Harris IS, Mak TW. Regulation of cancer cell metabolism. *Nat Rev Cancer*. 2011;11:85–95. doi:10.1038/nrc2981
14. Sena LA, Chandel NS. Physiological roles of mitochondrial reactive oxygen species. *Mol Cell*. 2012;48:158–167. doi:10.1016/j.molcel.2012.09.025
15. Gorrini C, Harris IS, Mak TW. Modulation of oxidative stress as an anticancer strategy. *Nat Rev Drug Discov*. 2013;12(12):931–947. doi:10.1038/nrd4002

16. Gabrielyan L, Trchounian A. Antibacterial activities of transient metals nanoparticles and membranous mechanisms of action. *World J Microbiol Biotechnol*. 2019;35(10):162. doi:10.1007/s11274-019-2742-6
17. Gabrielyan L, Hakobyan L, Hovhannisyan A, Trchounian A. Effects of iron oxide ($Fe_3O_4$) nanoparticles on Escherichia coli antibiotic-resistant strains. *J Appl Microbiol*. 2019;126 (4):1108–1116. doi:10.1111/jam.14214
18. Chen Q, Zhou J, Chen Z, Luo Q, Xu J, Song G. Tumor-specific expansion of oxidative stress by glutathione depletion and use of a fenton nanoagent for enhanced chemodynamic therapy. *ACS Appl Mater Interfaces*. 2019;11(34):30551–30565. doi:10.1021/acsami.9 b09323
19. Li J, Chen Y, Zeng L, et al. A nanoparticle carrier for co-delivery of gemcitabine and small interfering RNA in pancreatic cancer therapy. *J Biomed Nanotechnol*. 2016;12(8):1654–1666. doi:10.1166/jbn.2016. 2269
20. Wani KD, Kadu BS, Mansara P, et al. Synthesis, characterization and in vitro study of biocompatible cinnamaldehyde functionalized magnetite nanoparticles (CPGF Nps) for hyperthermia and drug delivery applications in breast cancer. *PLoS One*. 2014;9(9):e107315. doi:10.1371/journal.pone.0107315
21. Bonnet D, Dick JE. Human acute myeloid leukemia is organized as a hierarchy that originates from a primitive hematopoietic cell. *Nat Med*. 1997;3:730–737. doi:10.1038/nm0797-730
22. Bhardwaj G, Wu D, Baker DP, et al. Sonic hedgehog induces the proliferation of primitive human hematopoietic cells via BMP regulation. *Nat Immunol*. 2001;2:172–180. doi:10.1038/84282
23. Reya T, Morrison SJ, Clarke MF, et al. Stem cells, cancer, and cancer stem cells. *Nature*. 2001;41:105–111. doi:10.1038/ 35102167
24. Yang CP, Xiong F, Wang J, et al. Anti-ABCG2 monoclonal antibody in combination with paclitaxel nanoparticles against cancer stem-like cell activity in multiple myeloma. *Nanomedicine*. 2014;9:45–60. doi:10.2217/nnm.12.216
25. Shi F, Yang F, He X, et al. Inhibitory effect of epirubicin-loaded lipid microbubbles with conjugated anti-ABCG2 antibody combined with therapeutic ultrasound on multiple myeloma cancer stem cells. *J Drug Target*. 2016;24(1):34–46. doi:10.3109/1061186X. 2015.1052075
26. Dou J, Pan M, Wen P, et al. Isolation and identification of cancer stem like cells from murine melanoma cell lines. *Cell Mol Immunol*. 2007;4:528–533.
27. Zhang H, Cai K, Wang J, et al. MiR-7, inhibited indirectly by lincRNA HOTAIR, directly inhibits SETDB1 and reverses the EMT of breast cancer stem cells by downregulating the STAT3 pathway. *Stem Cells*. 2014;32(11):2858–2868. doi:10.1002/stem.1795
28. Dave B, Granados-Principal S, Zhu R, et al. Targeting RPL39 and MLF2 reduces tumor initiation and metastasis in breast cancer by inhibiting nitric oxide synthase signaling. *PANAS*. 2014;111:8838–8843. doi:10.1073/pnas.1320769111
29. Chen J, Wang J, Zhang Y, et al. Observation of ovarian cancer stem cell behavior and investigation of potential mechanisms of drug resistance in three-dimensional cell culture. *J Biosci Bioeng*. 2014;118(2):214–222. doi:10.1016/j.jbiosc.2014.01.008
30. Matsui W, Huff CA, Wang Q, et al. Characterization of clonogenic multiple myeloma cells. *Blood*. 2004;103:2332–2336. doi:10.1182/ blood-2003-09-3064
31. Shi F, Yang F, He X, et al. Induction of multiple myeloma cancer stem cell apoptosis using conjugated anti-ABCG2 antibody with epirubicin-loaded microbubbles. *Stem Cell Res Ther*. 2018;9:144. doi:10.1186/s13287-018-0885-2
32. Alhuthali HM, Bradshaw TD, Lim K-H, Kam T-S, Seedhouse CH. The natural alkaloid Jerantinine B has activity in acute myeloid leukemia cells through a mechanism involving c-Jun. *BMC Cancer*. 2020;20(1):629. doi:10.1186/s12885-020-07119-2
33. Sedlic F, Seiwerth F, Sepac A, et al. Mitochondrial ROS induce partial dedifferentiation of human mesothelioma via upregulation of NANOG. *Antioxidants (Basel)*. 2020;9(7):E606. doi:10.3390/ antiox9070606
34. Li F, Zhao F, Li M, et al. Decreasing new york esophageal squamous cell carcinoma 1 expression inhibits multiple myeloma growth and osteolytic lesions. *J Cell Physiol*. 2020;235(3):2183–2194. doi:10.1002/jcp.29128
35. Li M, Pan M, You C, et al. MiR-7 reduces the BCSC subset by inhibiting XIST to modulate the miR-92b/Slug/ESA axis and inhibit tumor growth. *Breast Cancer Res*. 2020;22:26. doi:10.1186/s13058-020-01264-z
36. Dou J, Wang Y, Wang J, et al. Antitumor efficacy induced by human ovarian cancer cells secreting IL-21 alone or combination with GM-CSF cytokines in nude mice model. *Immunobiology*. 2009;214 (6):392–483. doi:10.1016/j.imbio.2008.11.002
37. Zhang Y, Wang J, Ren M, et al. Gene therapy of ovarian cancer using IL-21-secreting human umbilical cord mesenchymal stem cells in nude mice. *J Ovarian Res*. 2014;7(1):8. doi:10.1186/1757-2215-7-8
38. Wang J, Zhou D, He X, et al. Effect of downregulated β-catenin on cell proliferative activity, the sensitivity to chemotherapy drugs and tumorigenicity of ovarian cancer cells. *Cell Mol Biol (Noisy-Le-Grand)*. 2011;57 Suppl:OL1606–13.
39. Yang C, Xiong F, Dou J, et al. Target therapy of multiple myeloma by PTX-NPs and ABCG2 antibody in a mouse xenograft model. *Oncotarget*. 2015;6(29):27714–27724. doi:10.18632/oncotarget.4663
40. Sawyers CL, Gishizky ML, Quan S, Golde DW, Witte ON. Propagation of human blastic myeloid leukemias in the SCID mouse. *Blood*. 1992;79 (8):2089–2098. doi:10.1182/blood.V79.8.2089.2089
41. Ouyang L, Shen LY, Li T, et al. Inhibition effect of Oncostatin M on metastatic human lung cancer cells 95D in vitro and on murine melanoma cells B16BL6 in vivo. *Biomed Res*. 2006;27:197–202.
42. Yang C, Wang J, Chen D, et al. Paclitaxel-Fe3O4 nanoparticles inhibit growth of CD138- CD34- tumor stem-like cells in multiple myeloma-bearing mice. *Int J Nanomedicine*. 2013;8:1439–1449. doi:10.2147/IJN.S38447
43. Ayyanaar S, Balachandran C, Bhaskar RC, et al. ROS-responsive chitosan coated magnetic iron oxide nanoparticles as potential vehicles for targeted drug delivery in cancer therapy. *Int J Nanomedicine*. 2020;15:3333–3346. doi:10.2147/IJN.S249240
44. Rahimi M, Karimian R, Noruzi EB, et al. Needle-shaped amphoteric calix[4]arene as a magnetic nanocarrier for simultaneous delivery of anticancer drugs to the breast cancer cells. *Int J Nanomedicine*. 2019;14:2619–2636. doi:10.2147/IJN.S194596
45. Cheng C, Li C, Zhu X, Han W, Li J, Lv Y. Doxorubicin-loaded $Fe_3O_4$ -ZIF-8 nano-composites for hepatocellular carcinoma therapy. *J Biomater Appl*. 2019;33(10):1373–1381. doi:10.1177/0885328 219836540
46. Bensaad K, Cheung EC, Vousden KH. Modulation of intracellular ROS levels by TIGAR controls autophagy. *EMBO J*. 2009;28 (19):3015–3026. doi:10.1038/emboj.2009.242
47. Chen YF, Wu SN, Gao JM, et al. The antioxidant, anti-inflammatory, and neuroprotective properties of the synthetic chalcone derivative AN07. *Molecules*. 2020;25(12):2907. doi:10.3390/molecules25122907
48. Shokoofeh N, Moradi-Shoeili Z, Naeemi AS, Jalali A, Hedayati M, Salehzadeh A. Biosynthesis of $Fe_3O_4$@Ag nanocomposite and evaluation of its performance on expression of norA and norB efflux pump genes in ciprofloxacin-resistant staphylococcus aureus. *Biol Trace Elem Res*. 2019;191(2):522–530. doi:10.1007/s12011-019-1632-y
49. Wu Q, He Z, Wang X, et al. Cascade enzymes within self-assembled hybrid nanogel mimicked neutrophil lysosomes for singlet oxygen elevated cancer therapy. *Nat Commun*. 2019;10:240. doi:10.1038/ s41467-018-08234-2

50. Cho JH, Kim K, Kim SA, et al. Deubiquitinase OTUD5 is a positive regulator of mTORC1 and mTORC2 signaling pathways. *Cell Death Differ*. 2020. doi:10.1038/s41418-020-00649-z
51. Benfield CT, MacKenzie F, Ritzefeld M, et al. Bat IFITM3 restriction depends on S-palmitoylation and a polymorphic site within the CD225 domain. *Life Sci Alliance*. 2020;3:e201900542.
52. Gan CP, Sam KK, Yee PS, et al. IFITM3 knockdown reduces the expression of CCND1 and CDK4 and suppresses the growth of oral squamous cell carcinoma cells. *Cell Oncol*. 2019;42:477–490. doi:10.1007/s13402-019-00437-z